Atomic-Scale Interface Structure in Domain Matching Epitaxial BaBiO₃ Thin Films Grown on SrTiO₃ Substrates

Lei Jin,* Michael Zapf, Martin Stübinger, Martin Kamp, Michael Sing, Ralph Claessen, and Chun-Lin Jia

The electronic structures of BaBiO₃ (BBO) thin films grown on SrTiO₃ substrates are found to be thickness dependent. The origin of this behavior remains under debate and has been suggested to be attributed to the structural and compositional modifications at the BBO/SrTiO₃ interface during the first stage of film growth. Though a wetting layer with thickness of ≈ 1 nm has been experimentally identified at the interface, details on the microstructures of such a layer and their effect on the subsequent film growth are lacking so far, particularly at the atomic scale. Herein, atomic-resolution scanning transmission electron microscopy is used to study the interface structure of a 30 nm-thick BBO film grown on an Nb-doped SrTiO₃ (STO) substrate through domain matching epitaxy. An interfacial δ-Bi₂O₃ (BO)-like phase with fluorite structure is identified, showing a layer-by-layer spacing of ≈ 3.2 Å along the growth direction. The orientation relationship between the BO-like phase and surrounding perovskites (P) is found to be $<001>_{BO}||<001>_P$ and $<110>_{BO}||<100>_P$. The presence of the BO-like phase results in two types of interfaces, i.e., a coherent BO/STO and a semicoherent BBO/BO interface. Thickness variations are observed in the BO-like layer, resulting in the formation of antiphase domains in the BBO films.

In addition to single crystals, high-quality thin films provide an ideal playground to investigate the essential structural and

Dr. L. Jin, Prof. C.-L. Jia
Ernst Ruska-Centre for Microscopy and Spectroscopy with Electrons
Forschungszentrum Jülich GmbH
Jülich 52428, Germany
E-mail: l.jin@fz-juelich.de

Dr. M. Zapf, M. Stübinger, Dr. M. Kamp, Prof. M. Sing, Prof. R. Claessen
Physikalisches Institut and Würzburg-Dresden Cluster of Excellence
ct.qmat
Universität Würzburg
Würzburg 97074, Germany

Prof. C.-L. Jia
The School of Electronic and Information Engineering
Xi'an Jiaotong University
Xi'an 710049, China

The ORCID identification number(s) for the author(s) of this article can be found under https://doi.org/10.1002/pssr.202000054.

physical properties of materials,[1,2] due to the possibility of tuning their structural parameters and chemical compositions. Such films are also of great importance for studies of materials with emergent phenomena,[3–5] induced by the presence of interfaces (either to a substrate or to neighboring layers as in a multilayer or superlattice system), which adds more degrees of freedom for controlling the materials properties, e.g., by lattice strain or interface/surface manipulations. For example, in the case of BaBiO₃ (BBO) thin films, if a BiO₂-termination is achieved, the pseudocubic $(001)_P$ surface, considered as one type of interface (hereafter the subscript "P" denotes perovskite), has been predicted to host a 2D electron gas.[6] Its origin is neither associated with the presence of oxygen vacancies nor with a polar discontinuity and thus differentiates itself from the prototypical LaAlO₃/SrTiO₃ case.[3]

BBO, a well-known parent material for the high-T_C superconducting compounds Ba$_{1-x}$K$_x$BiO₃ and BaPb$_{1-x}$Bi$_x$O₃,[7,8] adopts a monoclinically distorted perovskite structure (space group: I2/m) at room temperature,[9,10] with a pseudocubic lattice constant of ≈ 4.36 Å (e.g., ICSD-67073). Recently, BBO was used as potential absorber for all-oxide solar cells and as photocatalyst for water reduction.[11–13] Within the pseudocubic cells of BBO, the BiO₆-octahedra show about 10° rotations[10] that can be described by the Glazer notation $a_P^- b_P^- c_P^0$,[14,15] whereas the Bi—O bond varies between 2.11 and 2.29 Å for adjacent octahedra leading to the so-called breathing mode distortion.[10]

Though considerable efforts have been made to understand the structures and physical properties of BBO, there is an ongoing debate about the origin of the breathing mode distortion. Early on, it was attributed to the formation of Bi³⁺ and Bi⁵⁺ charge order on the BiO₆-octahedra network, leading to the insulating (or semiconductor-like) ground state for undoped BBO.[9,16] Due to this charge disproportionation, the nominal valence state of BBO was described, in an ionic picture, as Ba²⁺Bi₀.₅³⁺Bi₀.₅⁵⁺O₃²⁻ (or Ba₂²⁺Bi³⁺Bi⁵⁺O₆²⁻ as in a double perovskite unit cell)[10,12] rather than Ba²⁺Bi⁴⁺O₃²⁻. Alternatively, it was argued that such a distortion is accompanied by a spatial condensation of hole pairs into local, molecular-like orbitals of A_{1g} symmetry composed of Bi-6s and O-2p$_\sigma$ atomic orbitals of collapsed BiO₆-octahedra, leaving Bi ions in a

ADVANCED
SCIENCE NEWS

www.advancedsciencenews.com

physica **pss** rrl
status solidi

www.pss-rapid.com

monovalent state throughout the lattice.[17–19] In addition, there are also inconsistencies in the reported bandgap values. For instance, theoretical calculations predict a 1.3[20] or 1.45 eV[18] direct bandgap, whereas the experimentally determined values show variations, viz. 1.66,[21] 1.9,[20,22] ≈2,[1] and 2.04 eV.[23]

To solve these problems and to further study doping-related effects (such as superconductivity, photocatalysis, and so on), high-quality BBO single crystals and thin films are demanded. In contrast to the studies on the synthesis of BBO single crystals,[19,24–26] reports on epitaxial growth of BBO thin films are limited. It has been shown that, aside from the growth on MgO substrates (lattice mismatch of ≈1.4%),[27,28] smooth and well-ordered BBO thin films can be deposited on $SrTiO_3$ substrates (lattice mismatch of ≈12%) through domain matching epitaxy[29–31] even without the use of buffer layers such as BaO and $BaCeO_3/BaZrO_3$.[32,33] BBO films can be further used as buffer layers for the stabilization of the energetically unfavorable, but electronically nontrivial perovskite phase in the Y—Bi—O system.[34] In addition, it was recently reported that the electronic structure of BBO shows a thickness dependence for films directly grown on $SrTiO_3$ substrates,[30,35] whose origin was attributed to the structural and compositional modifications at the $BBO/SrTiO_3$ interface.[35]

Although it was experimentally found that a wetting layer with thickness of about 1 nm might exist at the interface,[31,34,36] information on the detailed microstructures for such a layer and their role in the subsequent film growth is lacking, particularly at the atomic scale. For example, using high-angle annular dark-field (HAADF) scanning transmission electron microscopy (STEM) imaging, this interfacial layer was reported to possess a rock-salt structure, whose formation can decouple the substrate from the film, thus stabilizing the heterostructure.[34] However, it should be noted that the determination of the oxygen positions is of critical importance in distinguishing fluorites[37] from rock salts,[34] as both structures appear the same in the HAADF images (oxygen is invisible). So far, this distinction has not been achieved.

Herein, we study the interface of a 30 nm-thick BBO film grown directly on a TiO_2-terminated 0.05 wt% Nb-doped $SrTiO_3$ (STO) substrate through domain matching epitaxy. The quality of our BBO thin-film samples grown under identical conditions has been studied previously by X-ray diffraction and electron microscopy,[31] and is also exemplified by low-magnification HAADF STEM of the lamella investigated in this study (Figure S1, Supporting Information). Using atomic-resolution scanning transmission electron microscopy, we reveal an interfacial δ-Bi_2O_3 (BO)-like layer with fluorite structure. The orientation relationship between the BO-like phase and surrounding perovskites is found to be $<001>_{BO}||<001>_P$ and $<110>_{BO}||<100>_P$ (hereafter the subscript "BO" denotes the BO-like phase). The presence of the BO-like phase results in two interfaces, i.e., a coherent BO/STO and a semicoherent BBO/BO interface, which has been also discussed by interface modeling. In addition, the influence of this interfacial BO-like layer on the subsequent growth of the BBO film is demonstrated.

Figure 1a,b shows the atomically resolved HAADF images of the BBO thin film and the corresponding atomic structures, projected along the perovskite $<100>_P$ and $<110>_P$ directions, respectively. Due to the large difference in atomic numbers Z between Ba ($Z = 56$) and Bi ($Z = 83$), the individual atomic
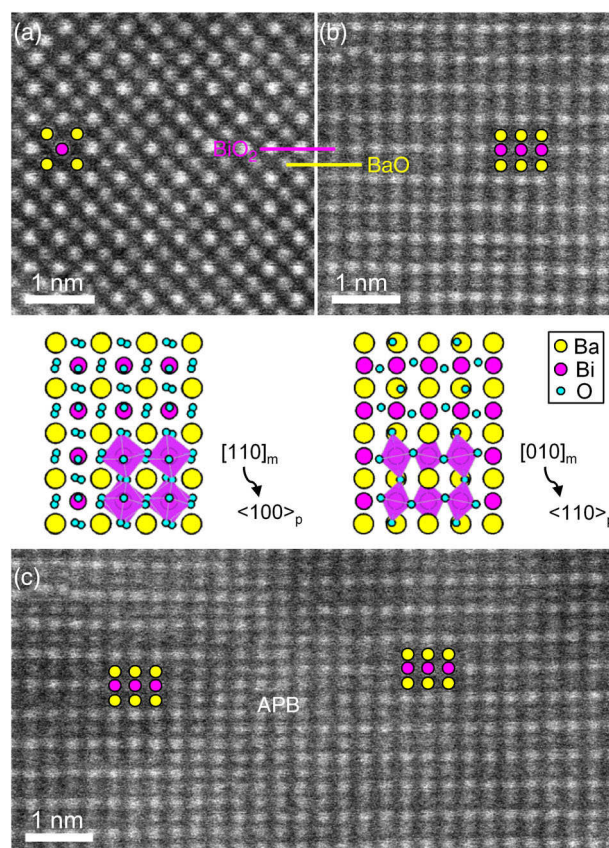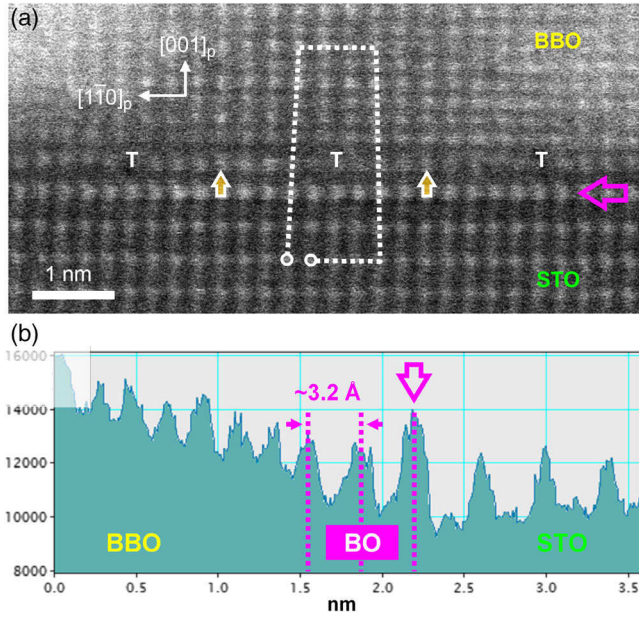

Figure 1. HAADF images and corresponding atomic models of the BBO film projected along the perovskite a) $<100>_P$ (|| monoclinic $[110]_m$) and b) $<110>_P$ (|| monoclinic $[010]_m$) directions. c) HAADF image showing two antiphase domains.

columns associated with Ba and Bi can be clearly distinguished according to the apparent image intensity, which are indicated by yellow and magenta dots, respectively. The pure oxygen columns ($Z = 8$), however, are not visible in the HAADF image. In Figure 1c, an antiphase boundary (APB) is observed with a shift of half a unit cell along the growth direction between the two adjacent domains (see overlaid models). The intensity difference between Ba- and Bi-related columns is no longer evident at the APB due to overlap of the two domains with their boundary inclined to the viewing direction. This is a very common feature in the BBO film used in this study.

Figure 2a shows a very typical HAADF image of the interface area taken along the $<110>_P$ direction, whereas Figure 2b shows the corresponding image intensity profile (averaged along the $[1\bar{1}0]_P$ direction) plotted along the $[001]_P$ direction. Based on the abrupt intensity change, the interface between the film and STO substrate can be determined, as is marked by the magenta arrow. In the following, we call this interface as the lower interface.

Three misfit dislocations (MDs) are indicated by the label "T" in Figure 2a. The separation between them amounts to about 2.48 nm for the observed BBO/STO interface, meaning that eight BBO $(1\bar{1}0)_P$ planes are in registry with nine STO $(1\bar{1}0)_P$ planes at the interface (see lattice planes between the two vertical arrows). This leads to the so-called domain matching epitaxy growth.[31]

ADVANCED SCIENCE NEWS
www.advancedsciencenews.com

pss rrl
physica status solidi
www.pss-rapid.com

Figure 2. a) HAADF image showing the interface structure. The viewing direction is $[110]_P$. The indicated Burgers circuit shows that the vector of MDs is $\bar{a}_P[\bar{1}10]/2$, where $\bar{a}_P \approx 4.13$ Å is the mean lattice constant of the unit cells of BBO and STO. b) Corresponding image intensity profile (averaged along the $[1\bar{1}0]_P$ direction) plotted along the $[001]_P$ direction, showing the presence of a δ-Bi$_2$O$_3$ (BO)-like interface layer. For details see text.

Further examinations reveal that the termination plane of the MDs is not right at the film/substrate interface (lower interface), but two atomic planes above, which is called stand-off behavior.[38] A similar phenomenon was observed in a recent

study.[34] Hereafter, we denote the dislocation-defined plane as the upper interface.

The domain matching epitaxy can be well understood within a near coincidence site lattice (CSL) model proposed for large-misfit systems,[39] as the natural lattice misfit between BBO and STO is ≈12%. In this model, given that n spacings of BBO bulk match ($n \pm 1$) spacings of STO at the interface, the unit cell dimension of the interface superstructure requires $n \times d_{BBO} = (n \pm 1) \times d_{STO}$ for an arbitrary interface structure. Here, $d_{BBO} \approx 4.36/\sqrt{2} = 3.08$ Å and $d_{STO} \approx 3.91/\sqrt{2} = 2.76$ Å for the $(1\bar{1}0)_P$ planes, therefore, only ($n + 1$) is valid. This yields $n \approx 8.6$, which is slightly larger than the value $n = 8$ measured from the APB-free interface areas. As the STO substrate is thought to be rigid, the reduction in n therefore necessitates an in-plane lattice expansion of the BBO film from the bulk value to ≈4.39 Å (according to $\sqrt{2} \times 2.76 \times 9/8$ Å by supposing that the in-plane lattice parameter $a_P = b_P$). This is consistent to the measured value reported in the study by Zapf et al.[31] for the same sample used. The minimum CSL misfit F, as defined by $1 - ((n + 1) \times d_{STO})/(n \times d_{BBO})$, approaches zero. All of the results are indicative of the formation of a semicoherent BBO/STO interface, which is energetically favorable.

In addition, we note an interface wetting layer in Figure 2, as evidenced by the unexpected lattice spacing, i.e., ≈3.2 Å, in the intensity profile. This value is much larger than the values for half of the unit cells of BBO and STO. The wetting layer is found to be very sensitive to the Ga ion beam milling, which usually leads to the local thickness reduction or sample amorphization before HAADF imaging (Figure S1, Supporting Information).

To understand the structure of the interface wetting layer, we further magnified the coherent parts that are located between two MD cores (e.g., positions marked by vertical arrows in Figure 2a). The images are shown in **Figure 3**a,b, respectively, for
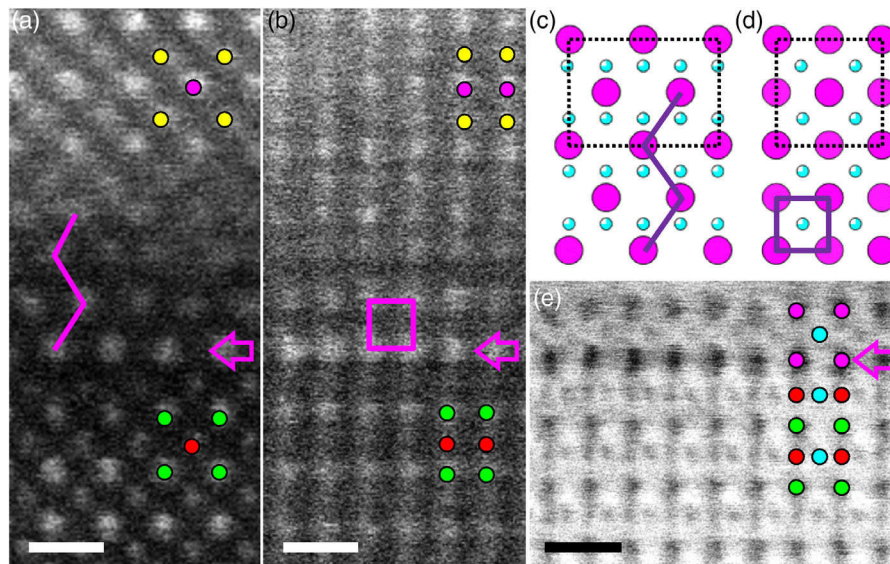
Figure 3. Magnified HAADF images from the coherent parts between two MDs, showing the atomic configurations of the interface wetting layer along a) $<100>_P$ and b) $<110>_P$. The wetting layer in (a) shows reduced intensity due to the local thickness reduction caused by preferential ion beam milling. c,d) Atomic models of δ-Bi$_2$O$_3$ projected along the $<110>_{BO}$ and $<100>_{BO}$ directions, respectively. e) ABF image taken from the BO/STO interface along $<110>_P||<100>_{BO}$. All atomic columns, including O, are imaged. (Bi: magenta, Ba: yellow, Sr: green, Ti/Nb: red, O: cyan). Scale bar: 0.5 nm. For details see text.

projections along the $<100>_P$ and $<110>_P$ directions of BBO. Considering the Z-contrast of the atomic columns (which is related to the chemical element) together with their arrangement (see zigzag line in Figure 3a and rectangle in Figure 3b) in the interface structure, one can deduce that the interface wetting layer possesses a δ-Bi$_2$O$_3$-like structure with a fluorite configuration. This is evident from the comparison with the corresponding projections of δ-Bi$_2$O$_3$, as shown in Figure 3c,d, which match our findings almost perfectly. Inconsistent with a recent report,[34] the interfacial layer was reported to possess a rock-salt structure based on the HAADF image alone. The orientation relationship between the interface BO-like layer and surrounding perovskites (i.e., STO and BBO) is found to be $<001>_{BO}||<001>_P$ and $<110>_{BO}||<100>_P$.

From Figure 3d, one can also see that the heavy cations (i.e., Bi, magenta dots) in the fluorite structure are no longer aligned in the same columns with anions (i.e., O, cyan dots) in the $<100>_{BO}$ projection, in contrast to the rock-salt structure. The fluorite structure can be directly recognized from our atomic resolution annular bright-field (ABF) image (Figure 3e), which reveals all atomic columns including O. However, it is still challenging to determine the exact composition of the interface layer, because of its extreme sensitivity to the electron beam. This leads to a failure when using any spectroscopic technique that is available in a transmission electron microscope.

Based on these results, we construct a rigid model to understand the interface structure. The model consists of three phases, viz. Nb-STO, BO, and BBO, in a fully relaxed strain condition (**Figure 4**a). In this model, we assume that all the phases are stoichiometric. For clarity, the Nb dopants are not considered, and the oxygen atoms are not displayed. From experiment (Figure 3a,b), we infer that the thickness of the interface BO-like layer varies from 2 to 4 Bi layers throughout the entire film. Nevertheless, we use two layers in the model shown in Figure 4 without loss of generality.

In Figure 4a, it is shown that due to the stand-off behavior of the dislocations the lower BO/STO interface becomes coherent. In contrast, the upper BBO/BO interface is semicoherent due to the MDs, as is predicted by the CSL theory. This interface further dissociates into two parts: the coherent part (marked by dashed ellipses) and the misfit part, where the MDs are terminated (marked by the labels "T"). The configurations at both upper and lower interfaces indeed match our experimental observations shown in Figure 2a.

To better understand the interface structure, we project the interface area as indicated by the bracket in Figure 4a along the interface normal (i.e., growth direction). This projection is shown in Figure 4b. It is evident that the coherent part (denoted "terrace" in the study by Dholabhai et al.[40]) can be further grouped into two types according to the local stacking sequence along the growth direction. Specifically, if we take the atom positions in STO (i.e., X-site corresponds to Sr and Y-site to Ti) as a reference, the stacking sequence can be described as $...X_{Sr}Y_{Ti}–X_{Bi}Y_{Bi}–Y_{Ba}X_{Bi}...$ for type I and $...X_{Sr}Y_{Ti}–X_{Bi}Y_{Bi}–X_{Ba}Y_{Bi}...$ for type II terraces, as shown by the dotted lines in Figure 4c.

We further note that the observed thickness variations of the BO-like layer (see, e.g., Figure 3) can be considered as surface steps (of a new "substrate") for the subsequent growth of the BBO films. As the Bi–Bi layer distance is about half of the perovskite unit cell, the presence of these surface steps inevitably leads
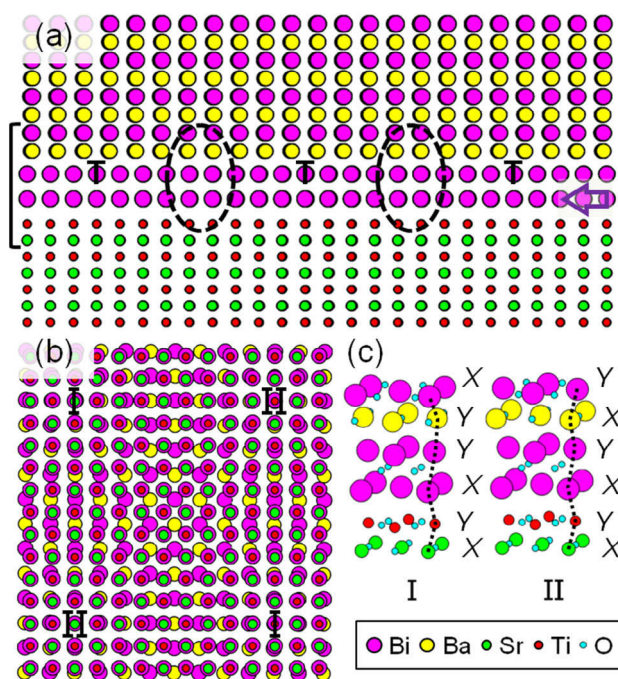
Figure 4. a) Rigid structure model consisting of STO, BO, and BBO in a fully relaxed strain condition. The arrow marks the BO/STO interface (lower interface). The coherent and misfit parts are indicated by dashed ellipses and labels "T," respectively. b) Model projected along the normal of the interface plane (in this view, STO is above BBO). Only one unit cell of STO and one of BBO next to the interface are shown for clarity. Two types of coherent parts ("terraces") are recognized. c) Local stacking sequences at type I and type II terraces. The sequences are $...X_{Sr}Y_{Ti}–X_{Bi}Y_{Bi}–Y_{Ba}X_{Bi}...$ for type I and $...X_{Sr}Y_{Ti}–X_{Bi}Y_{Bi}–X_{Ba}Y_{Bi}...$ for type II terraces, as shown by the dotted lines. For clarity, the Nb dopants are not considered and the oxygen atoms in (a) and (b) are not displayed.
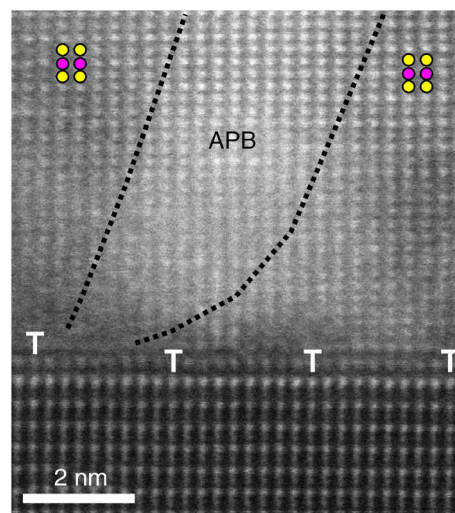
Figure 5. HAADF image showing the relationship between the nucleation position of antiphase domains in the BBO film and the thickness variation of the interfacial BO layer. The termination planes of MDs are marked by labels "T." The position of the inclined APB is marked by the dotted lines.

to the formation of antiphase domains in the BBO film. This can be clearly seen in the image of **Figure 5**, where the interface layer changes from 3 (left) to 2 (right) Bi layers, as evaluated on the basis of the lattice coherency at both the BBO/BO and BO/STO interfaces (see also the positions of the MDs marked by "T"). Similar observations were also reported in the study by Bouwmeester et al.,[34] however, no direct evidences were provided. By controlling the thickness variations of the interface layer (e.g., by deliberately depositing a BO-like layer prior to the BBO growth), the film quality may be further improved.

Yet, there are still several issues that are not well understood. First, supposing that BO ($a_{BO} = 5.655$ Å) is fully strained and maintains its cell volume on STO, the out-of-plane Bi—Bi layer distance would be expected to amount to ≈ 2.98 Å, which is $\approx 7\%$ less than the observed value in Figure 2b. One possible reason for this deviation is the interface relaxations (or reconstructions) induced by the local electrostatic interactions, which are reported to be very sensitive to the nearest neighbor arrangements between cations and anions across the interface.[40] In addition, for a full understanding, the following aspects also need to be considered: 1) The direct B_{Bi}–B_{Ba} connections at type I terraces (Figure 4c) may cause strong repulsive interactions, leading to a lattice expansion; 2) Given that all atomic sites of interface BO are occupied, the local composition can be deduced as —Bi_2—O_4—Bi_2—. To keep charge neutralization, this may result in a reduction of the Bi valence (from Bi^{3+} to Bi^{2+}, with the ionic radius r changing from 1.03 Å for Bi^{3+} to 1.61 Å for Bi^{2+})[41] or the introduction of Bi vacancies (with respect to O) to maintain a Bi^{3+} state as in BO; 3) the polar discontinuities at the TiO_2—Bi and Bi—BaO interfaces require additional charge compensation, which, due to the coupling between lattice and polarization as in ferroelectrics and other systems,[4,42] may lead to an expansion of the lattice; and 4) a possible intermixing of Ba^{2+} ($r = 1.35$ Å)[43] and Sr^{2+} ($r = 1.18$ Å)[43] cannot be excluded. To fully resolve these problems, atomistic simulations, as, e.g., used in the case of a similar MgO/STO semicoherent system (mismatch: $\approx 7\%$),[40] should be considered in the future.

We finally note that similar phases have been widely reported in thin films of $Bi_4Ti_3O_{12}$[44] and $BiFeO_3$ when they were grown at high growth rates and/or at high oxygen pressures.[37,45–47] This implies that the formation of the BO-like phase is probably a common phenomenon in the growth of Bi-containing perovskites associated with the high volatility of Bi. In addition, the stoichiometry of the target, film thickness, and deposition temperature affect the phase purity as well.[44–47] Further systematic investigations are therefore needed.

In summary, the structure of the interfaces between domain matching epitaxial BBO films and STO substrates has been studied using atomic-resolution scanning transmission electron microscopy and related modeling. We find that the interface is mediated by a δ-Bi_2O_3-like layer with fluorite structure, which shows $<001>_{BO}||<001>_P$ and $<110>_{BO}||<100>_P$ orientation relationships with reference to the surrounding perovskite film. The presence of the BO-like phase results in two types of interfaces occurring in parallel/simultaneously, i.e., coherent BO/STO and semicoherent BBO/BO interfaces. Thickness variations are observed in the interface BO-like layer, resulting in the formation of antiphase domains in the BBO films. As δ-Bi_2O_3 was reported to have metal-like electrical

characteristics,[44] its contribution to the thickness-dependent conductivity of BBO films has to be considered.

Experimental Section

BBO films were deposited on TiO_2-terminated 0.05 wt% Nb-doped STO substrates by pulsed laser deposition. The detailed procedure is described in previous studies.[31] The thickness of the film used in this study was about 30 nm. Cross-sectional specimens for STEM investigations were prepared by focused Ga ion beam milling on a Dual-Beam System (FEI Helios Nanolab), followed by a gentle surface cleaning using a 500 eV Ar ion beam in a Fischione Nanomill 1040 system. The HAADF and ABF STEM imaging were conducted on an FEI Titan G^2 80-200 ChemiSTEM microscope equipped with a high-brightness field-emission gun, an spherical aberration correction system for the probe forming system and a super-X energy dispersive X-ray spectroscopy attachment.[48] The microscope was operated at 200 kV with spatial resolution better than 80 pm. The convergence semiangle for STEM imaging was ≈ 22 mrad, whereas the collection semiangle was 11–21 mrad for ABF imaging and 70–200 mrad for HAADF imaging. Structural modeling was carried out using VESTA software.[49] (Further details of the crystal structure investigation(s) may be obtained from the Fachinformationszentrum Karlsruhe, 76344 Eggenstein-Leopoldshafen (Germany), on quoting the depository number ICSD-67073.)

Supporting Information

Supporting Information is available from the Wiley Online Library or from the author.

Conflict of Interest

The authors declare no conflict of interest.

[1] H. Sato, S. Tajima, H. Takagi, S. Uchida, *Nature* **1989**, *338*, 241.

[2] S. R. Burns, D. Sando, B. Xu, B. Dupé, L. Russell, G. Deng, R. Clements, O. H. C. Paull, J. Seidel, L. Bellaiche, N. Valanoor, C. Ulrich, *NPJ Q. Mater.* **2019**, *4*, 18.

[3] A. Ohtomo, H. Y. Hwang, *Nature* **2004**, *427*, 423.

[4] R. J. Zeches, M. D. Rossell, J. X. Zhang, A. J. Hatt, Q. He, C.-H. Yang, A. Kumar, C. H. Wang, A. Melville, C. Adamo, G. Sheng, Y.-H. Chu,

J. F. Ihlefeld, R. Erni, C. Ederer, V. Gopalan, L. Q. Chen, D. G. Schlom, N. A. Spaldin, L. W. Martin, R. Ramesh, *Science* **2009**, *326*, 977.

[5] L. Wang, Q. Feng, Y. Kim, R. Kim, K. H. Lee, S. D. Pollard, Y. J. Shin, H. Zhou, W. Peng, D. Lee, W. Meng, H. Yang, J. H. Han, M. Kim, Q. Lu, T. W. Noh, *Nat. Mater.* **2018**, *17*, 1087.

[6] V. Vildosola, F. Güller, A. M. Llois, *Phys. Rev. Lett.* **2013**, *110*, 206805.

[7] L. F. Mattheiss, E. M. Gyorgy, D. W. Johnson Jr, *Phys. Rev. B* **1988**, *37*, 3745.

[8] R. J. Cava, B. Batlogg, J. J. Krajewski, R. Farrow, L. W. Rupp Jr, A. E. White, K. Short, W. F. Peck, T. Kometani, *Nature* **1988**, *332*, 814.

[9] D. E. Cox, *Solid State Commun.* **1976**, *19*, 969.

[10] B. J. Kennedy, C. J. Howard, K. S. Knight, Z. Zhang, Q. Zhou, *Acta Crystallogr., Sect. B: Struct. Sci.* **2006**, *62*, 537.

[11] A. S. Chouhan, E. Athresh, R. Ranjan, S. Raghavan, S. Avasthi, *Mater. Lett.* **2018**, *210*, 218.

[12] J. Ge, W.-J. Yin, Y. Yan, *Chem. Mater.* **2018**, *30*, 1017.

[13] A. M. Huerta-Flores, D. Sánchez-Martínez, M. del Rocío Hernández-Romero, M. E. Zarazúa-Morín, L. M. Torres-Martínez, *J. Photochem. Photobiol., A* **2019**, *368*, 70.

[14] A. M. Glazer, *Acta Crystallogr., Sect. B: Struct. Sci.* **1972**, *28*, 3384.

[15] P. M. Woodward, *Acta Crystallogr., Sect. B: Struct. Sci.* **1997**, *53*, 32.

[16] C. M. Varma, *Phys. Rev. Lett.* **1988**, *61*, 2713.

[17] K. Foyevtsova, A. Khazraie, I. Elfimov, G. A. Sawatzky, *Phys. Rev. B* **2015**, *91*, 121114(R).

[18] N. C. Plumb, D. J. Gawryluk, Y. Wang, Z. Ristić, J. Park, B. Q. Lv, Z. Wang, C. E. Matt, N. Xu, T. Shang, K. Conder, J. Mesot, S. Johnson, M. Shi, M. Radović, *Phys. Rev. Lett.* **2016**, *117*, 037002.

[19] S. Balandeh, R. J. Green, K. Foyevtsova, S. Chi, O. Foyevtsov, F. Li, G. A. Sawatzky, *Phys. Rev. B* **2017**, *96*, 165127.

[20] H. Namatame, A. Fujimori, H. Takagi, S. Uchida, F. M. F. de Groot, J. C. Fuggle, *Phys. Rev. B* **1993**, *48*, 16917.

[21] T. Hatakeyama, S. Takeda, F. Ishikawa, A. Ohmura, A. Nakayama, Y. Yamada, A. Matsushita, J. Yea, *J. Ceram. Soc. Jpn.* **2010**, *118*, 91.

[22] S. Tajima, S. Uchida, A. Masaki, H. Takagi, K. Kitazawa, S. Tanaka, S. Sugai, *Phys. Rev. B* **1987**, *35*, 696.

[23] M. Khraisheh, A. Khazndar, M. A. Al-Ghouti, *Int. J. Energy Res.* **2015**, *39*, 1142.

[24] K. Kobayashi, T. Mizokawa, A. Ino, J. Matsuno, A. Fujimori, H. Samata, A. Mishiro, Y. Nagata, F. M. F. de Groot, *Phys. Rev. B* **1991**, *59*, 15100.

[25] T. Nishio, H. Minami, H. Uwe, *Physica C* **2001**, *357–360*, 376.

[26] Y. Imai, T. Noji, M. Kato, Y. Koike, in *AIP Conf. Proc.*, American Institute of Physics, Orlando, FL, USA **2006**, Vol. *850*, pp. 667–668.

[27] E. S. Hellman, E. H. Hartford, E. M. Gyorgy, *Appl. Phys. Lett.* **1991**, *58*, 1335.

[28] K. Inumaru, H. Miyata, S. Yamanaka, *Phys. Rev. B* **2008**, *78*, 132507.

[29] A. Gozar, G. Logvenov, V. Y. Butko, I. Bozovic, *Phys. Rev. B* **2007**, *75*, 201402(R).

[30] G. Kim, M. Neumann, M. Kim, M. D. Le, T. D. Kang, T. W. Noh, *Phys. Rev. Lett.* **2015**, *115*, 226402.

[31] M. Zapf, M. Stübinger, L. Jin, M. Kamp, F. Pfaff, A. Lubk, B. Büchner, M. Sing, R. Claessen, *Appl. Phys. Lett.* **2018**, *112*, 141601.

[32] T. Makita, H. Abe, *Jpn. J. Appl. Phys.* **1997**, *36*, L96.

[33] H. G. Lee, Y. Kim, S. Hwang, G. Kim, T. D. Kang, M. Kim, M. Kim, T. W. Noh, *APL Mater.* **2016**, *4*, 126106.

[34] R. L. Bouwmeester, K. de Hond, N. Gauquelin, J. Verbeeck, G. Koster, A. Brinkman, *Phys. Status Solidi RRL* **2019**, *13*, 1800679.

[35] M. Zapf, S. Elsässer, M. Stübinger, P. Scheiderer, J. Geurts, M. Sing, R. Claessen, *Phys. Rev. B* **2019**, *99*, 245308.

[36] J. Kim, J. Mun, B. Kim, H. G. Lee, D. Lee, T. H. Kim, S. Lee, M. Kim, S. H. Chang, T. W. Noh, *Phys. Rev. Mater.* **2019**, *3*, 113606.

[37] L. Jin, P. X. Xu, Y. Zeng, L. Lu, J. Barthel, T. Schulthess, R. E. Dunin-Borkowski, H. Wang, C. L. Jia, *Sci. Rep.* **2017**, *7*, 39698.

[38] W. Mader, G. Necker, in *Metal-Ceramic Interfaces* (Eds: M. Rühle, A. G. Evans, M. F. Ashby, J. P. Hirth), Pergamon Press, Oxford **1990**.

[39] L. Lu, J. Wang, H. Zheng, D. Zhao, R. Wang, J. Gui, *J. Mater. Res.* **2012**, *27*, 1895.

[40] P. P. Dholabhai, G. Pilania, J. A. Aguiar, A. Misra, B. P. Uberuaga, *Nat. Commun.* **2014**, *5*, 5043.

[41] N. Plakida, *High-Temperature Cuprate Superconductors – Experiment, Theory, and Applications*, Springer Series in Solid-State Sciences, Vol. *166*, Springer, Berlin/Heidelberg, Germany **2010**.

[42] C. L. Jia, S. B. Mi, M. Faley, U. Poppe, J. Schubert, K. Urban, *Phys. Rev. B* **2009**, *79*, 081405(R).

[43] R. D. Shannon, *Acta Crystallogr. A* **1976**, *32*, 751.

[44] M. Alexe, J. F. Scott, C. Curran, N. D. Zakharov, D. Hesse, A. Pignolet, *Appl. Phys. Lett.* **1998**, *73*, 1592.

[45] H. Liu, P. Yang, K. Yao, K. P. Ong, P. Wu, J. Wang, *Adv. Funct. Mater.* **2012**, *22*, 937.

[46] L. You, N. T. Chua, K. Yao, L. Chen, J. Wang, *Phys. Rev. B* **2009**, *80*, 024105.

[47] H. Béa, M. Bibes, A. Barthélémy, K. Bouzehouane, E. Jacquet, A. Khodan, J. P. Contour, S. Fusil, F. Wyczisk, A. Forget, D. Lebeugle, D. Colson, M. Viret, *Appl. Phys. Lett.* **2005**, *87*, 072508.

[48] Ernst Ruska-Centre for Microscopy and Spectroscopy with Electrons, *J. Large-Scale Res. Facil.* **2016**, *2*, A43.

[49] K. Momma, F. Izumi, *J. Appl. Crystallogr.* **2011**, *44*, 1272.